AIP | Journal of Applied Physics

Molecular beam epitaxy growth of high quality p-doped SnS van der Waals epitaxy on a graphene buffer layer

W. Wang, K. K. Leung, W. K. Fong, S. F. Wang, Y. Y. Hui et al.

Citation: J. Appl. Phys. **111**, 093520 (2012); doi: 10.1063/1.4709732
View online: http://dx.doi.org/10.1063/1.4709732
View Table of Contents: http://jap.aip.org/resource/1/JAPIAU/v111/i9
Published by the American Institute of Physics.

Molecular beam epitaxy growth of high quality p-doped SnS van der Waals epitaxy on a graphene buffer layer

W. Wang,[1] K. K. Leung,[1] W. K. Fong,[1] S. F. Wang,[1] Y. Y. Hui,[2] S. P. Lau,[2] Z. Chen,[3] L. J. Shi,[3] C. B. Cao,[3] and C. Surya[1,a)]
[1]*Department of Electronic and Information Engineering and Photonics Research Centre, The Hong Kong Polytechnic University, Hong Kong, People's Republic of China*
[2]*Department of Applied Physics, The Hong Kong Polytechnic University, Hong Kong, People's Republic of China*
[3]*Research Center of Materials Science, Beijing Institute of Technology, Beijing 100081, People's Republic of China*

(Received 29 January 2012; accepted 29 March 2012; published online 7 May 2012)

We report on the systematic investigation of optoelectronic properties of tin (IV) sulfide (SnS) van der Waals epitaxies (vdWEs) grown by molecular beam epitaxy (MBE) technique. Energy band simulation using commercial CASTEP code indicates that SnS has an indirect bandgap of size 0.982 eV. Furthermore, our simulation shows that elemental Cu can be used as a p-type dopant for the material. Growth of high quality SnS thin films is accomplished by MBE technique using graphene as the buffer layer. We observed significant reduction in the rocking curve FWHM over the existing published values. Crystallite size in the range of 2–3 μm is observed which is also significantly better than the existing results. Measurement of the absorption coefficient, α, is performed using a Hitachi U-4100 Spectrophotometer system which demonstrate large values of α of the order of 10^4 cm^{-1}. Sharp cutoff in the values of α, as a function of energy, is observed for the films grown using a graphene buffer layer indicating low concentration of localized states in the bandgap. Cu-doping is achieved by co-evaporation technique. It is demonstrated that the hole concentration of the films can be controlled between 10^{16} cm^{-3} and 5×10^{17}cm^{-3} by varying the temperature of the Cu K-cell. Hole mobility as high as 81 cm^{2}V^{-1}s^{-1} is observed for SnS films on graphene/GaAs(100) substrates. The improvements in the physical properties of the films are attributed to the unique layered structure and chemically saturated bonds at the surface for both SnS and the graphene buffer layer. Consequently, the interaction between the SnS thin films and the graphene buffer layer is dominated by van der Waals force and structural defects at the interface, such as dangling bonds or dislocations, are substantially reduced. © *2012 American Institute of Physics*. [http://dx.doi.org/10.1063/1.4709732]

I. INTRODUCTION

Two-dimensional metal chalcogenides are attractive materials for applications in a wide range of nano-electronic and optoelectronic devices. A number of devices had been reported in the past several years taking advantage of their unique layered structure and their electrical and optoelectronic properties.[1–6] Field effect transistors had been fabricated using hafnium oxide as the gate dielectric deposited on single-layer MoS_2 films by atomic layer deposition technique. Good device characteristics have been demonstrated with room-temperature mobility up to 200 cm^2/Vs and transconductance of 1 μSμm^{-1} were recorded.[1] These layered semiconductors are also touted as potential photovoltaic materials due to their high absorption coefficients with bandgaps ranging from around 1 eV to 2.2 eV.[7–9]

A unique characteristic of this class of materials is that the chalcogenide atoms are chemically saturated and, as a result, the inter-layer interaction along the crystallographic c-axis is mainly by the weak vdW force.[10,11] This type of materials is commonly referred as vdWEs. There are a number of important properties associated with this class of materials. First, it is believed that there is a much greater tolerance in the lattice mismatch both between the thin film and the substrate as well as between different constituent materials at the heterojunction.[12–14] Thus, a much wider choice of substrates can be used for the growth of high quality vdWEs. Furthermore, since the chalcogenide planes consist of saturated bonds as a result the heterojunctions may be totally free of dangling bonds. This will have significant implications on the properties of the devices as the interface states typically have critical impact on both the electrical and optoelectronic properties of the junctions: the Fermi level will not be pinned at the metal/semiconductor interface; trap assisted recombination will be substantially suppressed; and low-frequency noise will be significantly lowered.[15–17] Studies on conventional semiconductor devices have shown that device degradations can often be traced back to the material defects in the devices, thus the lowering of the interface states concentration in the material may have positive effects on the lifetimes of the devices.[18]

There has been a search for the right thin-film semiconductor materials, with high carrier mobilities and are

a)Author to whom correspondence should be addressed. Electronic mail: ensurya@polyu.edu.hk.

compatible with flexible substrates, for the development of new technologies such as flexible or wearable computers, large-area high-resolution displays, electronic paper, and flexible PV cells. Tin-based chalcogenides had drawn the attention of a number of groups as a candidate for such applications.[19–23] It was reported by Mitzi *et al.*[24,25] that tin di-sulfoselenide ($SnS_{2-x}Se_x$) thin films can be obtained by a highly cost-effective spin coating technique. However, the carrier mobilities obtained are typically very low using this technique. Other groups had investigated tin monosulfide (SnS) as a promising photovoltaic material.[21–23] Previous work showed that SnS is a p-type material with an indirect and a direct bandgap at ~1–1.1 eV and ~1.3–1.5 eV, respectively, and high absorption coefficient of $\sim 10^4$ cm^{-1}.[26–28] In addition, the constituent elements are both abundantly found in the earth's crust and non-toxic which makes SnS an excellent candidate for large-scale deployment.[29] SnS-based heterojunction photovoltaic cells (PVCs) have been fabricated by various techniques with CdS as the common choice for the n-type semiconductor.[8,22,30] However, to date the reported conversion efficiency of the SnS-based PVCs are still quite low in the range of ~1.3%.[31] Recent work by Ichimura showed that one of the reasons for such low cell efficiency may due to the large conduction band offset at the CdS/SnS heterojunction resulting in an energy barrier at the junction and thereby blocking the photogenerated carriers in the SnS layer.[32] It was suggested that the use of ZnO as the window material may partially alleviate this problem.[33]

Examination of the existing data on SnS-based PVCs indicate low values in both the open circuit voltages, V_{OC}, and short circuit current densities, J_{SC}.[22,32–34] This stipulates that, in addition to a large band offset at the heterojunction, material defects also play an important role in the poor conversion efficiencies of the devices. High defect density in the range of 10^{12} cm^{-2} and small grain size in the range of 0.092 μm for the as-deposited films by co-evaporation technique had been reported which improved to 0.12 μm after annealing at 200 °C for 3 hours.[35] Work by Boonsalee on epitaxial electrodeposited SnS layers demonstrate an average full width at half maximum (FWHM) of 3.16° for the XRD peak.[36] Such film qualities are far from what is needed for the development of PVCs with high conversion efficiencies. To date, little work has been done on the effects of the interface states on the conversion efficiency of the device. So far all the SnS-based PVCs reported in the literature relied on un-doped SnS layers which exhibit p-type conductivity arising from Sn vacancies.[22,29,32–34] Consequently, there is little to no control over the hole concentration and hence no back surface field can be implemented in the device structure to reduce the impact of the localized states at the SnS/electrode interface. To improve the cell efficiencies of SnS-based PVCs, it is important to optimize both the growth conditions to improve the crystallinity of the material and the device structure to enhance V_{OC} and J_{SC} of the device. To accomplish this one will need to establish a back surface field in the device to suppress the trap assisted recombination of the photo-generated carriers in the SnS absorber. It is also important to find a proper n-type material for the formation of the junction to facilitate efficient collection of the carriers.

In the following sections, we will report a novel growth process in which p-type SnS is deposited by MBE technique using graphene as a buffer layer. Significant improvements in both the crystallinity and optoelectronic properties of the materials are observed. We have also investigated extrinsic p-doping of the thin films by co-evaporation of Cu. Our results show that the hole concentration can be controlled over a wide range of values by varying the temperature of the Cu K-cell.

II. ENERGY BAND SIMULATION

SnS crystallizes in an orthorhombic structure (Pnma 62 space group) and form double layers that are perpendicular to the direction of the unit cell's largest axis. The unit cell contains 8 atoms organized in two adjacent double layers. The lattice parameters for SnS are $a = 3.987$ Å, $b = 11.200$ Å, and $c = 4.334$ Å.[37] Energy band calculations were carried out using a commercial CASTEP code. The electronic exchange correlation was treated using the generalized-gradient approximation (GGA) with the Perdew-Burke-Ernzerhof (PBE) form. The interactions between the ionic cores and the electrons were described by the ultra-soft pseudopotentials. Pseudoatomic calculations were performed for Sn $5s^2 5p^2$ and S $3s^2 3p^4$. The energy cutoff was set at 290 eV. For the charge density integration, we have used the $(1 \times 3 \times 3)$ k-point Monkhorst-Pack mesh. The atomic coordinates of all the atoms in the supercell $(2 \times 2 \times 2)$, that contain 64 atoms, were optimized without any symmetry constraint using the Broyden-Fletcher-Goldfarb-Shanno scheme. The convergence in energy and force was set at 2×10^{-5} eV/atom and 0.05 eV/Å, respectively.

Figures 1(a) and 1(b) show the dispersion of the energy bands in pure SnS and Cu doped SnS, respectively. From Fig. 1(a), the minima of the conduction band is located at Γ which does not coincide with the maxima of the valence

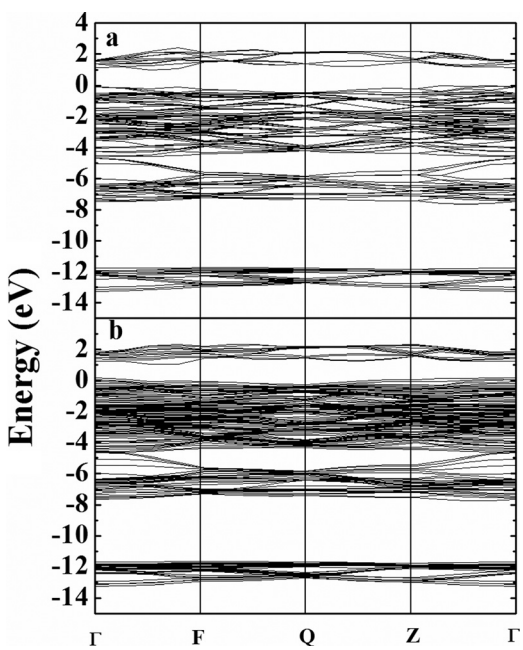

FIG. 1. Band structure of (a) pure SnS, $E_{ind} \approx 0.982$ eV and (b) Cu doped SnS, $E_{ind} \approx 0.864$ eV.

band. Thus, the indirect bandgap of SnS is 0.982 eV which is comparable with the experimental results.[26,38,39] By replacing a Sn atom with a Cu atom, the indirect bandgap decreased to 0.864 eV as shown in Fig. 1(b). Figure 2 shows the total density of states (DOS) of pure SnS and Cu doped SnS. According to the DOS spectra, the Fermi level of Cu-doped SnS is located at the top of the valence band indicative of a heavily p-doped material. These hole states near the top of the valence band come from the d states of Cu and p states of S by analyzing their partial density of states, which may result from the hybridization of the d states of Cu and p states of S. Considering the electronic configuration of Cu $3d^{10}4s^1$ and Sn $4d^{10}5s^25p^2$, Cu has less outer electrons than Sn suggesting that copper should be a p-type dopant for SnS.

III. EXPERIMENT AND RESULTS

We have performed systematic investigations on the growth of SnS thin films by MBE technique, using SnS as our starting material, on different substrates including soda lime glass, GaAs(100), and SiO_2. Scanning electron microscopy (SEM) and high resolution x-ray diffraction (HXRD) measurements were used to characterize the crystallinity of the material which was found to show strong dependencies on the substrate and the growth temperature. From the SEM results shown in Figs. 3 and 4, it is observed that at low substrate temperature, the grain size is much smaller than 1 μm for films grown on both glass and GaAs(100) substrates. Flake like structures with preferred growth perpendicular to the substrate are observed. For films grown on GaAs(100) substrates at $T_S = 400\,^{\circ}\mathrm{C}$ a much smoother surface was obtained with platelets of size $\sim$0.5 μm are observed. This is in contrast to films grown on glass in which rough surface morphology was observed at all substrate temperatures we tested (100 °C–400 °C). The experimental results on HXRD ω-scan of the (040) reflection are shown in Fig. 5. The sample deposited on glass at $T_S = 400\,^{\circ}\mathrm{C}$ demonstrates very

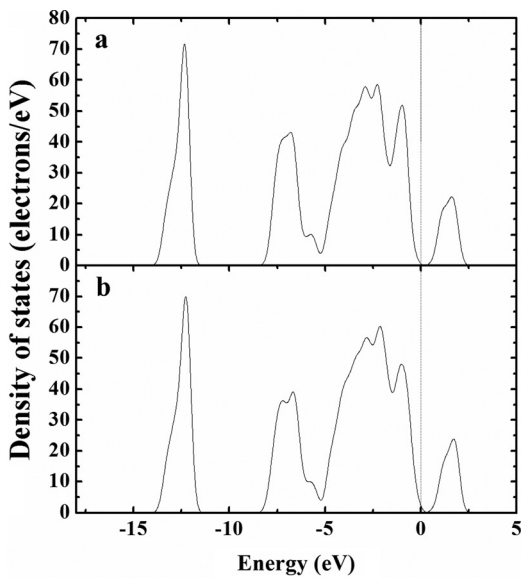

FIG. 2. Total density of state (DOS) of (a) pure SnS, $E_{ind} \approx 0.982$ eV, and (b) Cu doped SnS, $E_{ind} \approx 0.864$ eV. Dotted line is the Fermi level which is being used as the reference.

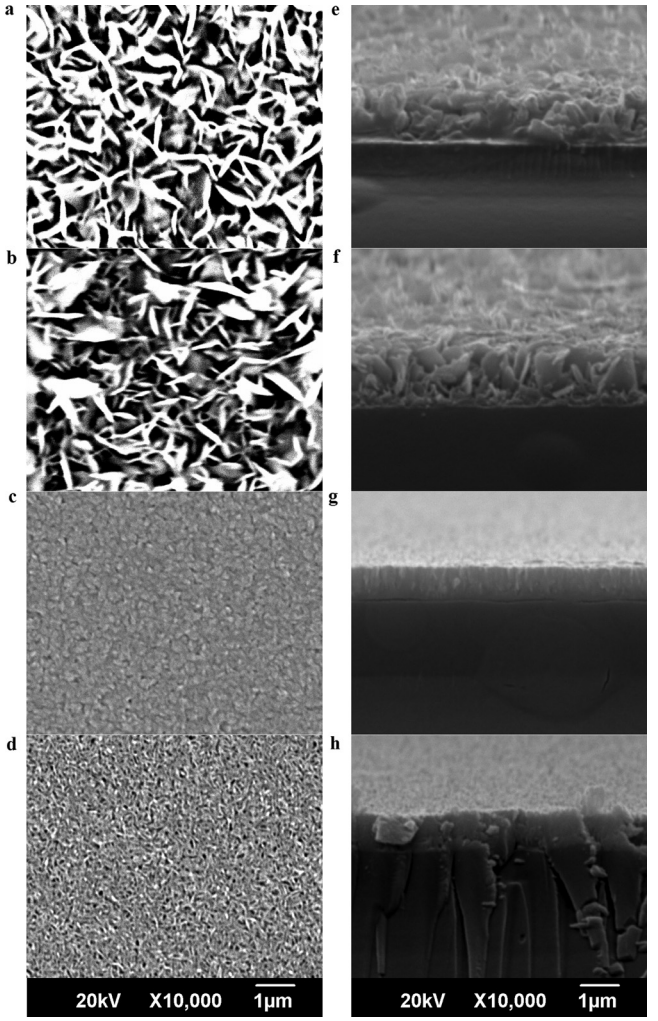

FIG. 3. Top view and cross-sectional SEM images of SnS deposited on glass at 400 °C (a and e); 300 °C (b and f); 200 °C (c and g); and 100 °C (d and h).

broad rocking curve signal as indicated by the solid squares in Fig. 5. Significant improvement in the crystallinity is observed from the SnS films grown on GaAs(100) substrates which exhibit a rocking curve FWHM of 2.96°, as indicated by the open squares in Fig. 5, and is comparable to the results reported by Boonsalee *et al.*[36]

Detailed characterizations of the optical properties of the films were performed using a Hitachi U-4100 Spectrophotometer system. The wavelength of the incident radiation was varied from 300 nm to 2500 nm and both the reflected and transmitted beams were measured to accomplish an accurate quantitative evaluation of α, which is related to the incident radiation energy, $h\nu$, by $\alpha \propto (h\nu - E_g \pm E_p)^r / h\nu$. For direct transition, $r = 1/2$ and $E_p = 0$ and for the case of allowed-indirect transition, $r = 2$ and E_p is nonzero and is equal to the energy of the phonon. The experimental data are shown in Fig. 6 below from which we were able to derive an indirect bandgap and a direct bandgap at 0.99 eV and 1.25 eV, respectively. The results are consistent with the published data.

P-doping of the material was achieved by incorporating Cu into the films by co-evaporation, and the doping

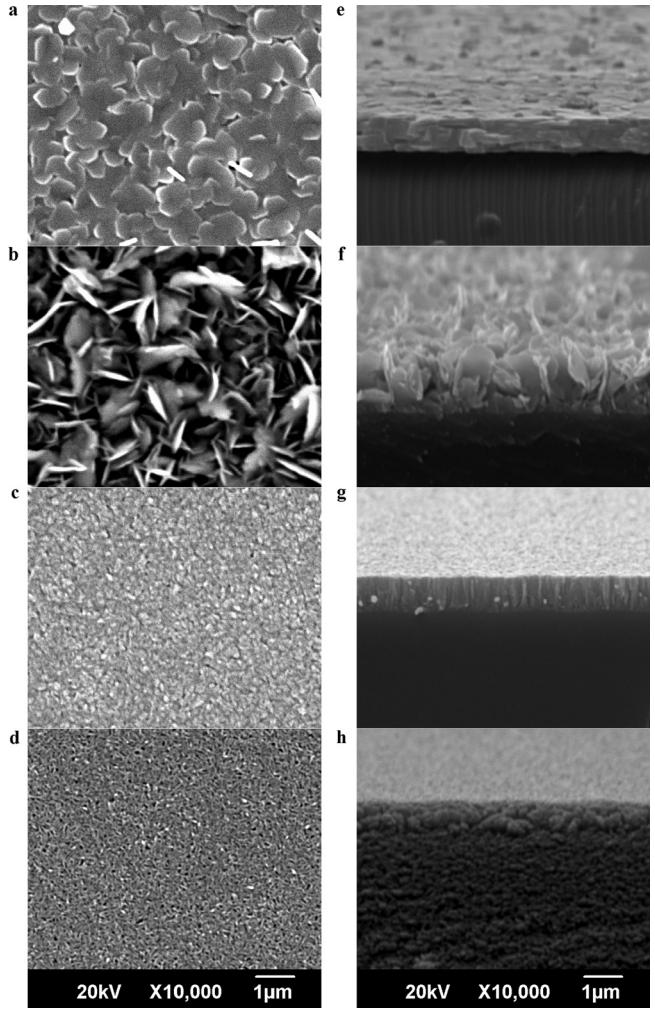

FIG. 4. Top view and cross-sectional SEM images of SnS deposited on GaAs(100) at 400 °C (a and e); 300 °C (b and f); 200 °C (c and g); and 100 °C (d and h).

concentration was varied by adjusting the temperature of the Cu K-cell. The hole mobility and hole concentration are represented by the open circles and open squares, respectively, in Fig. 7. The data clearly demonstrate good control of hole concentration in the film from $\sim 3 \times 10^{16}$ cm^{-3} to $\sim 4 \times 10^{17}$ cm^{-3} as the Cu K-cell temperature was varied from 1082 K to 1113 K. The results demonstrate clear

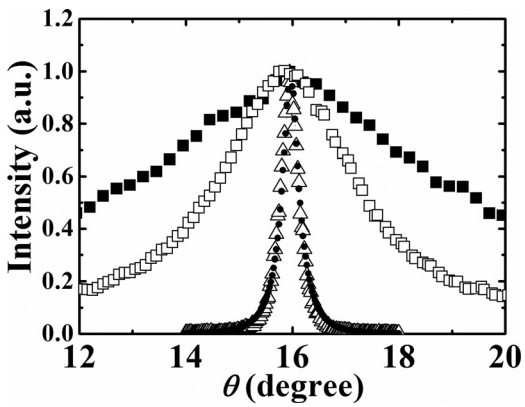

FIG. 5. XRD rocking curves for the (040) plane for SnS deposited on glass (solid squares); GaAs (open squares); Graphene/GaAs (open triangles); and Graphene/SiO_2/Si (solid circles).

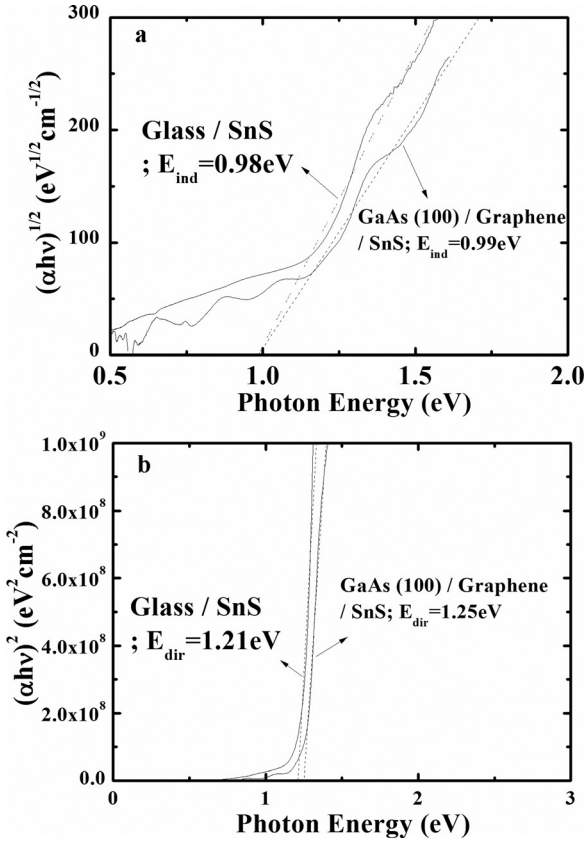

FIG. 6. Plot of $(\alpha h\nu)^{1/r}$ as a function of the photon energy.

correlation between the hole concentration and the Cu flux. Hall measurements were performed on SnS:Cu-on-GaAs films at $T_S = 400$ °C. A peak hole mobility of 25 cm^2 V^{-1} s^{-1} is observed at hole concentration $p \approx 1.4 \times 10^{17}$ cm^{-3}. This is substantially higher than the hole mobilities obtained for SnS films grown directly on glass which are typically in the single digit range. The general increase in the hole mobility with carrier concentration for $p < 10^{17}$ cm^{-3} is attributed to enhancement of the screening effect with increasing carrier concentration resulting in the lowering of Coulombic scattering rate. Further increase in the doping concentration resulted in the increase in material defect density leading to the corresponding degradation in the hole mobility.

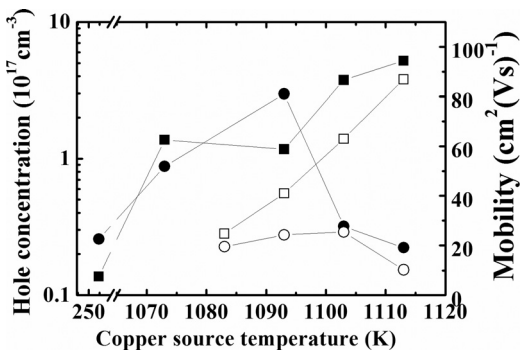

FIG. 7. Hole concentration and hall mobility as a function of copper source temperature for SnS deposited on Graphene/GaAs (solid squares and solid circles, respectively) and on GaAs (open squares and open circles, respectively).

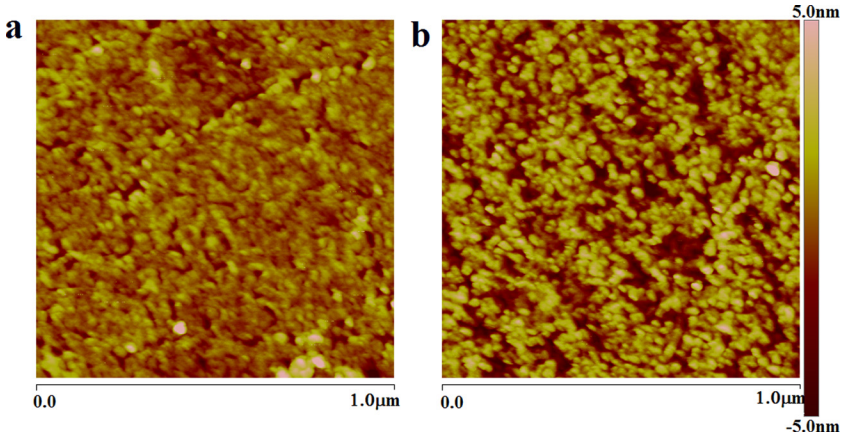

FIG. 8. AFM top view of the surface of SnS deposited on (a) graphene/GaAs with a rms surface roughness of 1.0 nm and (b) graphene/SiO_2/Si with a rms surface roughness of 1.4 nm.

From the experimental data, it is clear that while some improvements in the crystallinity of the SnS thin films have been accomplished over existing reported results but substantial further improvement is needed for the development of practical devices. It is noteworthy that the crystallinity of the film exhibited a strong dependence on the substrate. This contradicts to common belief that vdWEs have high tolerance on the lattice mismatch between the film and the substrate. It appears that, in practice, the interaction between the film and the underlying substrate in a quasi-vdWE system is probably much more significant than is expected.

To facilitate the growth of high quality SnS films on a foreign substrate we have investigated a novel growth technique in which graphene is used as the buffer layer between the substrate and the SnS layer. It is believed that the graphene layer should serve as an excellent buffer layer for the growth of vdWEs because, like the vdWEs, it is also layered structure consisting of saturated bonds and interacts with the substrate below and the deposited thin film above by van der Waals force. This should greatly reduce the impact of the substrate on the SnS films.

Double layer graphene films were grown on Cu foils (25-μm, Alfa Aesar) in a horizontal tube furnace.[40,41] The Cu foil was loaded into a quartz tube and then evacuated. The temperature of the furnace was then raised and stabilized at 1000 °C for 30 min with the flow of H_2/Ar gas maintained at a flow rate of 10 sccm/50 sccm. Then, CH_4 was introduced into the furnace for 10 min with a flow rate of 25 sccm. After the growth, the sample was allowed to cool down to room temperature under the flow of H_2/Ar gas. The surface of the graphene-on-Cu layer was spin-coated with poly-methyl methacrylate (PMMA) before the removal of the Cu foil by chemical etching using $FeCl_3$. After the Cu foil is dissolved, the PMMA coated graphene was cleaned with de-ionized water. The graphene film was then transferred to a GaAs(100) or SiO_2/Si substrate. After the transfer, the PMMA was removed using acetone. Figures 8(a) and 8(b) are AFM pictures of the graphene/GaAs and graphene/SiO_2/Si surfaces which indicate atomically smooth surface morphologies with rms surface roughness of 1.0 nm and 1.4 nm, respectively. The graphene/GaAs and graphene/SiO_2/Si substrates were then placed in an MBE chamber for the growth of SnS thin films at a substrate temperature of 400 °C. Cross sectional and top view SEM images were measured and the results are shown in Figs. 9(a) and 9(b) which demonstrate significant improvement in the surface morphology of the film. From the figure, a crystallite of size 2–3 μm was observed. To the best of our knowledge, this is close to an order of magnitude larger than the best reported results. Typical results on the HXRD rocking curve for the Cu-doped SnS thin films on Graphene/GaAs and Graphene/SiO_2/Si are represented by the open triangle and solid circles in Fig. 5, respectively, with a FWHM of around 0.37° which

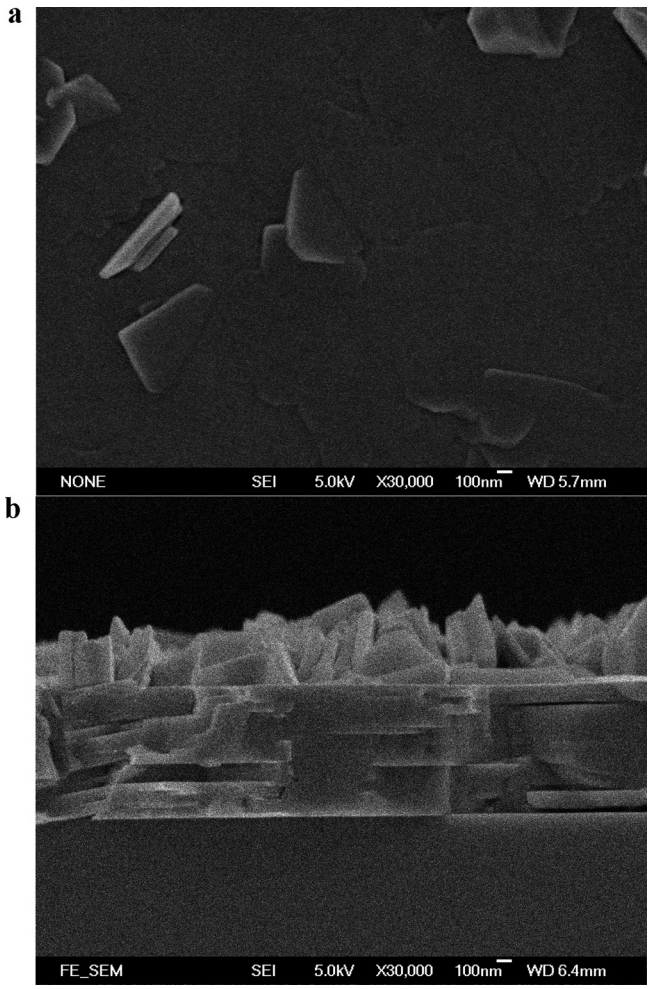

FIG. 9. SEM images indicating (a) planar view; and (b) cross-sectional view of SnS:Cu deposited on Graphene/GaAs at 400 °C.

demonstrates a significant improvement in the crystallinity of the film over the existing data. Furthermore, the results indicate that the impact of the substrate on the crystallinity of the film is significantly reduced when graphene is utilized as a buffer layer. To perform Hall measurements, the SnS films were mechanically exfoliated and transferred to an insulating Si substrate. The graphene was then removed from the debonded surface using nitrogen plasma cleaning for about 5 min. The experimental data on carrier concentration and hole mobility are indicated by solid squares and circles in Fig. 7, respectively, which exhibit a factor of 3.2 increase in the hole mobility over the maximum value achieved by SnS film grown directly on GaAs(100) substrate. Also, by systematically varying the Cu K-cell temperature from room temperature to 1113 K, the hole concentration can be controlled between $\sim 10^{16}$ cm^{-3} and $\sim 6\times 10^{17}$ cm^{-3}.

The α-SnS thin film can be described as a layered structure in which a unit cell consists of 4 Sn and 4 S atoms as shown in Fig. 10. The interface models for SnS (040) on GaAs (100) and SnS (040) on graphene are shown in Figs. 11(a) and 11(b), respectively. From Fig. 10(a), the S and As atoms are shown in yellow and red circles, respectively. By comparing the atomic distances between S atoms and As atoms, the lattice mismatch is determined to be −0.26% in the [100] direction and 8.42% in the [001] direction. From the prediction of this interface model, the [100] direction of SnS along [110] direction of GaAs is the most energetically favorable orientation for the growth of SnS on GaAs as this direction has a larger number of coincidence points than other directions. For the interface model of SnS (040) on graphene in Fig. 10(b), the S and C atoms are indicated by yellow and gray circles, respectively. The lattice mismatch is calculated to be 8.08% in the [100] direction and 1.74% in the [001] direction. Thus, the improvement in the crystallinity of the SnS films grown using graphene buffer layer cannot be explained by the improvement in the lattice match between the SnS film and graphene. Furthermore, it is expected that substantial stress will be observed in the film due to the large lattice mismatch.

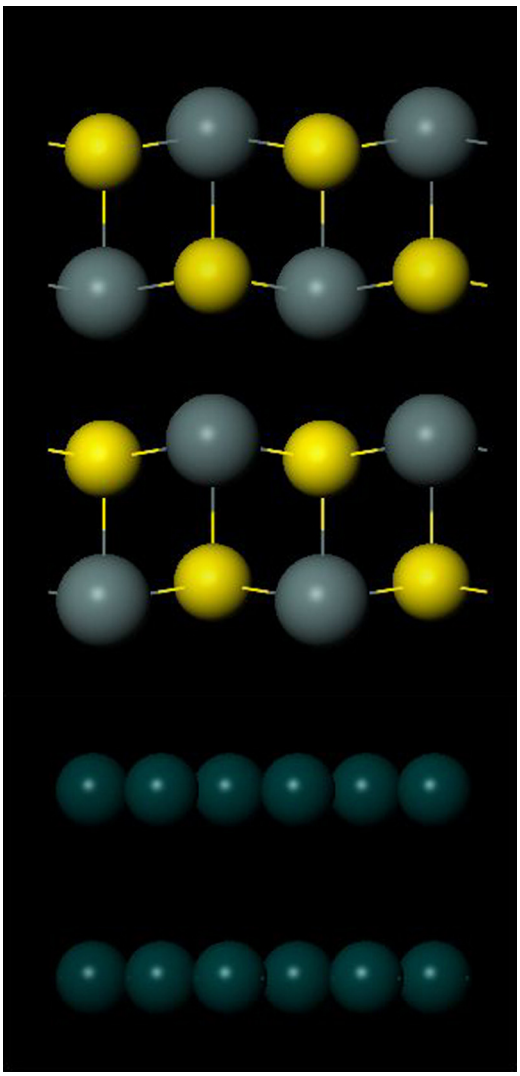

FIG. 10. Schematic cross section image of SnS on bi-layer Graphene.

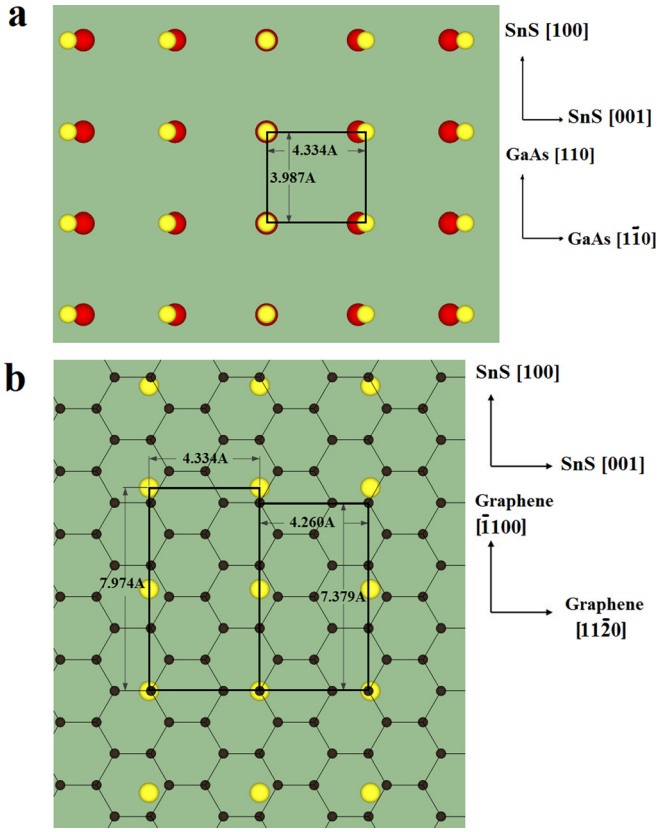

FIG. 11. Interface model of (a) SnS on GaAs(100). As and S atoms are in red and yellow color separately; and (b) SnS on Graphene. C and S atoms are in dark gray and yellow color, respectively.

To investigate the stress in the SnS films, we have conducted Raman spectroscopy measurement on the as-grown and the debonded SnS surfaces and the results are shown in Fig. 12. From the Raman spectra, four characteristic Raman lines can be observed at 96, 160, 189, and 220 cm^{-1}, which correspond to the longitudinal (LO = 9) and transverse (TO = 3) optical modes for bulk SnS single crystal.[42,43] This indicates that the SnS-on-graphene film is fully relaxed and is consistent with the idea that the interaction between SnS and the graphene buffer layer is dominated by a weak vdW force. Also, no significant peak shift and broadening is

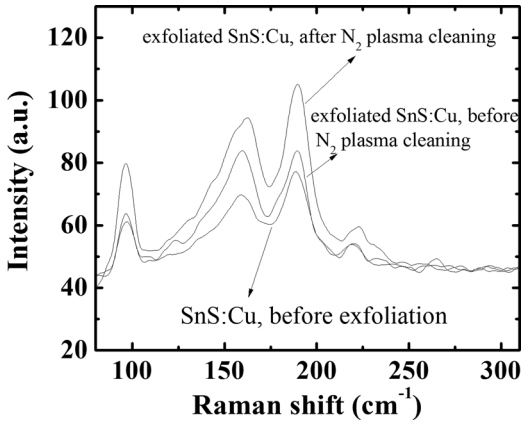

FIG. 12. Raman spectra of SnS films deposited on Graphene/GaAs.

observed in the Raman spectra before and after the exfoliation process, indicating nearly no change in the material strain is introduced by the exfoliation process.

Based on the experimental results, it can be concluded that the substantial improvement in the crystallinity for the SnS thin films arises from the weak vdW interaction between the SnS film and graphene buffer layer which facilitates the growth of fully relaxed SnS films despite significant lattice mismatch between SnS and graphene. The weak interaction between the Sn and S atoms with the graphene layer resulted in the high surface mobilities of the Sn and S atoms during film growth which is believed to account for the formation of large crystallites observed in the films.

IV. CONCLUSION

In conclusion, we have deposited high quality SnS films on GaAs(100) substrates by MBE using graphene as the buffer layer. Significant improvements in the FWHM of the rocking curve have been observed with a best value of 0.37°. Scanning electron microscopy shows that grain size of $\sim 3\,\mu$m is found in our films, which is roughly an order of magnitude larger than the reported values.[35] We have also investigated extrinsic p-doping of the films by co-evaporation of elemental Cu. Our results demonstrate good control of the hole concentration, between $\sim 10^{16}$ cm^{-3} and $\sim 6\times 10^{17}$ cm^{-3}, by varying the Cu flux from the K-cell. Hole mobility of 81 cm^2 V^{-1} s^{-1} is obtained at a hole concentration $p \approx 1.2 \times 10^{17}$ cm^{-3} which, to the best of our knowledge, is the highest value obtained in extrinsic SnS thin films.[44,45] Our results indicate that further improvement in the properties of the SnS can be achieved by optimizing the graphene transfer process to avoid formation of folds and pinholes in the layer.

ACKNOWLEDGMENTS

This work is supported in part by an RGC Grant (PolyU 5302/09E). Further support is provided by a Niche area grant of the Hong Kong Polytechnic University.

[1]B. Radisavljevic, A. Radenovic, J. Brivio, V. Giacometti, and A. Kis, "Single-layer MoS(2) transistors," Nat. Nanotechnol. **6**(3), 147–150 (2011).
[2]R. L. Withers and J. A. Wilson, "An examination of the formation and characteristics of charge-density waves in inorganic materials with special reference to the two-dimensional and one-dimensional transition-metal chalcogenides," J. Phys. C **19**(25), 4809–4845 (1986).
[3]A. Ayari, E. Cobas, O. Ogundadegbe, and M. S. Fuhrer, "Realization and electrical characterization of ultrathin crystals of layered transition-metal dichalcogenides," J. Appl. Phys. **101**(1), 014507 (2007).
[4]V. Podzorov, M. E. Gershenson, C. Kloc, R. Zeis, and E. Bucher, "High-mobility field-effect transistors based on transition metal dichalcogenides," Appl. Phys. Lett. **84**(17), 3301–3303 (2004).
[5]R. Spah, U. Elrod, M. Luxsteiner, E. Bucher, and S. Wagner, "Pn junctions in tungsten diselenide," Appl. Phys. Lett. **43**(1), 79–81 (1983).
[6]R. Spah, M. Luxsteiner, M. Obergfell, E. Bucher, and S. Wagner, "N-Mose2/P-Wse2 heterojunctions," Appl. Phys. Lett. **47**(8), 871–873 (1985).
[7]D. Avellaneda, M. T. S. Nair, and P. K. Nair, "Photovoltaic structures using chemically deposited tin sulfide thin films," Thin Solid Films **517**(7), 2500–2502 (2009).
[8]B. Ghosh, M. Das, R. Banerjee, and S. Das, "Fabrication of vacuum-evaporated SnS/CdS heterojunction for PV applications," Sol. Energy Mater. Sol. Cells **92**(9), 1099–1104 (2008).
[9]A. Sanchez-Juarez, A. Tiburcio-Silver, and A. Ortiz, "Fabrication of SnS(2)/SnS heterojunction thin film diodes by plasma-enhanced chemical vapor deposition," Thin Solid Films **480**, 452–456 (2005).
[10]D. Guay, W. M. R. Divigalpitiya, D. Belanger, and X. H. Feng, "Chemical bonding in restacked single-layer Mos(2) by x-ray-absorption spectroscopy," Chem. Mater. **6**(5), 614–619 (1994).
[11]P. Johari and V. B. Shenoy, "Tunable dielectric properties of transition metal dichalcogenides," Acs Nano **5**(7), 5903–5908 (2011).
[12]A. Koma, K. Sunouchi, and T. Miyajima, "Fabrication of ultrathin heterostructures with vanderwaals epitaxy," J. Vac. Sci. Technol. B **3**(2), 724–724 (1985).
[13]A. Koma, "Vanderwaals epitaxy—a new epitaxial-growth method for a highly lattice-mismatched system," Thin Solid Films **216**(1), 72–76 (1992).
[14]T. Ueno, H. Yamamoto, K. Saiki, and A. Koma, "Van der Waals epitaxy of metal dihalide," Appl. Surf. Sci. **113**, 33–37 (1997).
[15]O. Lang, R. Schlaf, Y. Tomm, C. Pettenkofer, and W. Jaegermann, "Single-crystalline Gase/Wse2 heterointerfaces grown by Van-Der-Waals epitaxy. 1. Growth-conditions," J. Appl. Phys. **75**(12), 7805–7813 (1994).
[16]O. Lang, Y. Tomm, R. Schlaf, C. Pettenkofer, and W. Jaegermann, "Single-crystalline Gase/Wse2 heterointerfaces grown by Van-Der-Waals epitaxy. 2. Junction characterization," J. Appl. Phys. **75**(12), 7814–7820 (1994).
[17]W. Jaegermann, C. Pettenkofer, and B. A. Parkinson, "Cu and Ag deposition on layered P-type Wse_2—approaching the Schottky limit," Phys. Rev. B **42**(12), 7487–7496 (1990).
[18]L. Sugiura, "Dislocation motion in GaN light-emitting devices and its effect on device lifetime," J. Appl. Phys. **81**(4), 1633–1638 (1997).
[19]W. M. Du, D. H. Deng, Z. T. Han, W. Xiao, C. Bian, and X. F. Qian, "Hexagonal tin disulfide nanoplatelets: A new photocatalyst driven by solar light," Cryst. Eng. Comm. **13**(6), 2071–2076 (2011).
[20]N. G. Deshpande, A. A. Sagade, Y. G. Gudage, C. D. Lokhande, and R. Sharma, "Growth and characterization of tin disulfide (SnS2) thin film deposited by successive ionic layer adsorption and reaction (SILAR) technique," J. Alloy Compd. **436**(1–2), 421–426 (2007).
[21]H. Noguchi, A. Setiyadi, H. Tanamura, T. Nagatomo, and O. Omoto, "Characterization of vacuum-evaporated tin sulfide film for solar-cell materials," Sol. Energy Mater. Sol. Cells **35**(1–4), 325–331 (1994).
[22]K. T. R. Reddy, N. K. Reddy, and R. W. Miles, "Photovoltaic properties of SnS based solar cells," Sol. Energy Mater. Sol. Cells **90**(18–19), 3041–3046 (2006).
[23]M. Ristov, G. Sinadinovski, M. Mitreski, and M. Ristova, "Photovoltaic cells based on chemically deposited p-type SnS," Sol. Energy Mater. Sol. Cells **69**(1), 17–24 (2001).
[24]D. B. Mitzi, M. Copel, and S. J. Chey, "Low-voltage transistor employing a high-mobility spin-coated chalcogenide semiconductor," Adv. Mater. **17**(10), 1285 (2005).
[25]D. B. Mitzi, L. L. Kosbar, C. E. Murray, M. Copel, and A. Afzali, "High-mobility ultrathin semiconducting films prepared by spin coating," Nature **428**(6980), 299–303 (2004).
[26]S. S. Hegde, A. G. Kunjomana, K. A. Chandrasekharan, K. Ramesh, and M. Prashantha, "Optical and electrical properties of SnS semiconductor crystals grown by physical vapor deposition technique," Physica B **406**(5), 1143–1148 (2011).

[27]A. Tanusevski and D. Poelman, "Optical and photoconductive properties of SnS thin films prepared by electron beam evaporation," Sol. Energy Mater. Sol. Cells **80**(3), 297–303 (2003).
[28]N. K. Reddy and K. T. R. Reddy, "Growth of polycrystalline SnS films by spray pyrolysis," Thin Solid Films **325**(1–2), 4–6 (1998).
[29]M. Ichimura, "Calculation of band offsets at the CdS/SnS heterojunction," Sol. Energy Mater. Sol. Cells **93**(3), 375–378 (2009).
[30]M. Gunasekaran and M. Ichimura, "Photovoltaic cells based on pulsed electrochemically deposited SnS and photochemically deposited US and Cd1-xZnxS," Sol. Energy Mater. Sol. Cells **91**(9), 774–778 (2007).
[31]K. Hartman, J. L. Johnson, M. I. Bertoni, D. Recht, M. J. Aziz, M. A. Scarpulla, and T. Buonassisi, "SnS thin-films by RF sputtering at room temperature," Thin Solid Films **519**(21), 7421–7424 (2011).
[32]A. M. Haleem and M. Ichimura, "Experimental determination of band offsets at the SnS/CdS and SnS/InS(x)O(y) heterojunctions," J. Appl. Phys. **107**(3), 034507 (2010).
[33]B. Ghosh, M. Das, P. Banerjee, and S. Das, "Fabrication of the SnS/ZnO heterojunction for PV applications using electrodeposited ZnO films," Semicond. Sci. Technol. **24**(2), 025024 (2009).
[34]Y. Wang, H. Gong, B. H. Fan, and G. X. Hu, "Photovoltaic behavior of nanocrystalline SnS/TiO(2)," J. Phys. Chem. C **114**(7), 3256–3259 (2010).
[35]N. K. Reddy, K. Ramesh, R. Ganesan, K. T. R. Reddy, K. R. Gunasekhar, and E. S. R. Gopal, "Synthesis and characterisation of co-evaporated tin sulphide thin films," Appl. Phys. A: Mater. Sci. Process. **83**(1), 133–138 (2006).
[36]S. Boonsalee, R. V. Gudavarthy, E. W. Bohannan, and J. A. Switzer, "Epitaxial electrodeposition of tin(II) sulfide nanodisks on single-crystal Au(100)," Chem. Mater. **20**(18), 5737–5742 (2008).
[37]H. Nozaki, M. Onoda, M. Sekita, K. Kosuda, and T. Wada, "Variation of lattice dimensions in epitaxial SnS films on MgO(001)," J. Solid State Chem. **178**(1), 245–252 (2005).
[38]W. Albers, C. Haas, and F. Vandermaesen, "The preparation and the electrical and optical properties of Sns crystals," J. Phys. Chem. Solids **15**(3–4), 306–310 (1960).
[39]B. Thangaraju and P. Kaliannan, "Spray pyrolytic deposition and characterization of SnS and SnS_2 thin films," J. Phys. D: Appl. Phys. **33**(9), 1054–1059 (2000).
[40]X. S. Li, W. W. Cai, J. H. An, S. Kim, J. Nah, D. X. Yang, R. Piner, A. Velamakanni, I. Jung, E. Tutuc, S. K. Banerjee, L. Colombo, and R. S Ruoff, "Large-area synthesis of high-quality and uniform graphene films on copper foils," Science **324**(5932), 1312–1314 (2009).
[41]K. M. Borysenko, J. T. Mullen, X. Li, Y. G. Semenov, J. M. Zavada, M. B. Nardelli, and K. W. Kim, "Electron-phonon interactions in bilayer graphene," Phys. Rev. B **83**(16), 161402(R) (2011).
[42]H. R. Chandrasekhar, R. G. Humphreys, U. Zwick, and M. Cardona, "Ir and raman-spectra of 4–6 compounds Sns and Snse," Phys. Rev. B **15**(4), 2177–2183 (1977).
[43]P. M. Nikolic, L. Miljkovic, P. Mihajlovic, and B. Lavrencic, "Splitting and coupling of lattice modes in layer compound Sns," J. Phys. C Solid State **10**(11), L289–L292 (1977).
[44]S. A. Zhang and S. Y. Cheng, "Thermally evaporated SnS:Cu thin films for solar cells," Micro. Nano Lett. **6**(7), 559–562 (2011).
[45]M. Devika, N. K. Reddy, K. Ramesh, K. R. Gunasekhar, E. S. R. Gopal, and K. T. R. Reddy, "Low resistive micrometer-thick SnS: Ag films for optoelectronic applications," J. Electrochem. Soc. **153**(8), G727–G733 (2006).